# Thermodynamic analysis of novel methanol polygeneration systems for greenhouses

Elie Antar[*,a], and Etienne Robert[b]

[a]Department of Mechanical Engineering, Polytechnique Montréal, Montréal, Québec, H3T 1J4, Canada (elie.antar@polymtl.ca) ORCID: 0000-0002-7519-8643

[b]Department of Mechanical Engineering, Polytechnique Montréal, Montréal, Québec, H3T 1J4, Canada (etienne.robert@polymtl.ca)

## Abstract

This work presents the modeling and thermodynamic analysis of two novel small-scale polygeneration systems that are capable of simultaneously converting residual biomass to methanol (MeOH), electricity, heat and a $CO_2$-rich stream for agricultural greenhouses. The first system is based on a downdraft gasifier, while the second relies on a dual fluidized bed (DFB) gasifier. Both configurations leverage the $H_2$, $O_2$, and electricity generation capabilities of reversible solid oxide cells (RSOCs). The Aspen Plus process simulator is used to model the thermodynamic performance of the proposed polygeneration systems, which operate at total efficiencies ranging from 83.9 to 85.0%. From a biofuel and electrical efficiency perspective, the system based on a DFB gasifier is superior, providing the added benefit of enabling carbon capture and storage, as a $N_2$-free stream with a molar purity exceeding 90% $CO_2$ is generated, which could be readily liquefied or sequestered.

**Keywords:** Polygeneration systems; Methanol; Carbon dioxide; Biomass gasification; Reversible fuel cells

## Declarations

**Funding:** The authors are grateful for the funders of this work: The Trottier Energy Institute (Trottier scholarship and project grant), and the Natural Sciences and Engineering Research Council of Canada (NSERC), [PGSD3 - 546588 - 2020].

**Conflicts of interest/Competing interests:** The authors declare that they have no known competing financial interests or personal relationships that could have appeared to influence the work reported in this paper.

**Availability of data and material:** Not applicable

**Code availability:** Not applicable

**Authors' contributions:** Elie Antar: Conceptualization, Methodology, Software, Validation, Formal analysis, Writing – Original Draft, Writing - Review & Editing, Visualization. Etienne Robert: Conceptualization, Formal analysis, Resources, Writing - Review & Editing, Supervision, Funding acquisition.

**Ethics approval:** Not applicable

**Consent to participate:** Not applicable

**Consent for publication:** Not applicable

[*] Corresponding author Email: elie.antar@polymtl.ca

## 1. Introduction

The agricultural sector is currently heavily reliant on costly and unecological products derived from fossil fuels for its energy-intensive activities, and contributes approximately 10% of the total greenhouse gas (GHG) emissions in Canada [1]. According to the Report on Energy Supply and Demand [2], agricultural activities consume around 6.7% of the total refined petroleum products used in the country. Farmers mainly depend on diesel fuel and gasoline for transportation and powering machinery. Moreover, in temperate climates such as Canada, heating typically represents 70-85% of the total energy expenses of greenhouses [3], with fuel oil and natural gas highly relied on. Canadian agricultural facilities also use 1.9% of the total electricity consumed in the country [4] for artificial lighting and powering electrical machinery. High-purity carbon dioxide is another resource highly demanded in greenhouses since its concentration in ambient air is too low for optimum crop growth, particularly during the day time when it is around 150 ppm [5]. A $CO_2$-rich stream is often injected into the greenhouse atmospheres to attain the optimal $CO_2$ concentration range of 700-1000 ppm, which has shown to enhance crop yield by 20 to 60% [6].

Residual lignocellulosic biomass, a potentially carbon neutral and renewable energy resource [7], is abundant in agricultural areas. Its use in greenhouses is currently mostly limited to biomass boilers, which in addition to their emission indicators being on par with hard coal [8], are typically only able to provide part of the required heat, with the peak thermal load along with the locally required transportation fuel, electricity, and $CO_2$ being covered by fossil-based products, as mentioned earlier. The reliance of farmers on these resources can be greatly minimized, and their energy sustainability can be considerably enhanced if gasification-based polygeneration systems are deployed in agricultural settings to harness the potential of the local energy resources.

Polygeneration systems are suitable for decentralized applications such as greenhouses as they can offer high overall thermodynamic efficiencies [9], which can remain essentially unaffected by the choice of operating pressures. This is a considerable advantage since for the synthesis of common storable biofuels such as methanol or dimethyl ether, the high operating pressure range of 50 – 80 bar needed for maximum yield [10,11] would impose serious safety consideration when implemented in a greenhouse. A safer operating pressure range of 20 – 30 bar causes a significant drop in biofuel yield, but this is compensated in polygeneration systems by: 1) using the unconverted syngas output of the biofuel reactors for the generation of electricity needed by the

greenhouse, and 2) directly using the generated heat from the exothermic biofuel reactors and the residual off-gas burners to meet the large heat demands of the greenhouse. This, and the fact that biomass transportation costs are minimized since the plants are installed next to the renewable biomass resources [12] have the potential to outweigh the additional equipment costs associated with polygeneration plants when compared with traditional heating approaches, making this an attractive option for greenhouse applications.

Studies in the literature of biomass gasification-based systems, which are largely based on steady state thermodynamic modelling, target a broad range of potential applications, nonetheless, the specific needs of greenhouses remain largely unaddressed. For instance, single output electricity/biofuel plants are heavily investigated, where using a downdraft gasifier coupled with a 2.5 kW internal combustion engine (ICE), Chaves et al. [13] reported a 16.5% biomass-to-electricity efficiency. Sara et al. [14] analyzed a 100 kW dual fluidized bed (DFB) gasifier-based system for $H_2$ production, and reported an efficiency ranging between 46-50%. The co-generation of heat and power from biomass is also commonly discussed. Sadegh-Vaziri and Bäbler [15] modelled a biomass system consisting of a fluidized bed gasifier and a solid oxide fuel cell (SOFC) that powered a gas turbine by feeding it with the unreacted syngas, and reported a total efficiency of 56% (electrical and thermal efficiencies of 20.4% and 35.6%, respectively). The tri-generation concept of electricity, biofuel, and heat has also been studied, but to a significantly lower extent. Clausen et al. [16] showed that tri-generation can yield very high overall efficiencies reaching 87-88%, by thermodynamically modelling two systems that produced either methanol (MeOH) or dimethyl ether (DME) as a biofuel. However, no studies were found on polygeneration systems designed to produce simultaneously the four products demanded for greenhouses and the surrounding agricultural activities.

The goal of this paper is to present and thermodynamically analyze two novel polygeneration systems capable of converting residual biomass to MeOH, electricity, heat and a $CO_2$-rich stream for greenhouses. The proposed systems mainly differ in the gasification stage, where a downdraft gasifier is used in the first system, while a DFB gasification approach is adopted in the second. The paper first discusses the system components chosen and their layouts, followed by the modelling approach implemented using the Aspen Plus process simulator. The energy flow

diagrams and parametric analysis are then presented in the results section, followed by a comparison of the energetic performances of both systems.

## 2. Methodology

### 2.1. General design choices

#### 2.1.1. Feedstock

Wood chips is the selected biomass feedstock for this study since it is widely available in agricultural settings and is commonly used in biomass conversion systems studies [17,18]. Its characteristics is shown in Table 1.

**Table 1: Characteristics of wood chips.**

| | ***Wood chips*** |
|---|---|
| ***Ultimate analysis (wt% dry basis)*** | |
| ***C*** | 50.6 |
| ***H*** | 6.5 |
| ***N*** | 0.2 |
| ***O*** | 42 |
| ***S*** | 0 |
| ***Proximate analysis (wt% dry basis)*** | |
| ***Moisture*** | 45 |
| ***FC*** | 19.2 |
| ***VM*** | 80.1 |
| ***Ash*** | 0.7 |
| ***LHV (MJ/kg wet basis)*** | 12.1 |
| ***HHV (MJ/kg wet basis)*** | 14 |

#### 2.1.2. Biofuel

MeOH is the liquid biofuel considered useful for greenhouses in this work as it can be readily stored, transported [19], and can completely substitute gasoline in ICEs with minor modifications [20]. In fact, compared to gasoline, MeOH has a higher octane number (107 vs 98), a wider flammability range, and burns cleaner [21]. One of the most important parameters for MeOH synthesis from biomass-derived syngas, besides the operating reactor pressure, is the $H_2$/CO ratio

which is usually kept at 2 [22]. It has been shown that enriching the $H_2$ content in syngas has the potential of increasing the amount of produced MeOH by up to 150% [23]. A solid oxide electrolysis cell (SOEC) running on internally generated electricity and steam is selected for $H_2$ syngas enrichment upstream the MeOH reactor in both of the proposed systems.

#### 2.1.3. Carbon dioxide

The choice of incorporating a SOEC is also motivated by the pure $O_2$ stream that is generated during the electrolysis process. This stream can play a key role in producing the high-purity $CO_2$ stream for the greenhouse atmosphere. After the oxy-gasification stage, and following the conversion of the resulting $N_2$-free syngas to biofuel and electricity, the leftover stream is mainly diluted with $CO_2$ and $H_2O$ [24], and can be burned at low temperatures without generating $NO_x$, yielding an exhaust suitable for greenhouse $CO_2$ enrichment. SOECs also contribute to higher overall system efficiencies compared to conventional air separation units (ASUs), as was demonstrated by Zhang et al. [25] who reported a total system efficiency increase from 47.9% to 59.1% after replacing an ASU with a SOEC in a biomass to MeOH plant. Butera et al. [26] also reached similar conclusions after integrating a SOEC into a system that converts biomass and electricity into MeOH.

#### 2.1.4. Electricity

Another attractive feature of SOECs exploited in this study is their ability to operate in reverse mode, as SOFCs, generating electricity for greenhouses efficiently from syngas with very low pollutants emissions [27]. Several experimental studies have been published recently reporting successful operation of 800-850˚C SOFC units fed with syngas from biomass gasifiers [28–30]. The added energy value of using SOFCs instead of conventional heat engines was highlighted by other investigations. A 7.3 percentage points increase in system efficiency was obtained by Minutillo et al. [31] after replacing a micro gas turbine (MGT) with a SOFC in a small-scale combined heat and power (CHP) system based on biomass gasification.

### 2.2. Downdraft gasifier-based system

The first system considered relies on a 1 bar downdraft gasifier, a simple gasification approach suitable for small-scale applications (10 kW to 1 MW) [32]. Figure 1 shows a schematic representation of the system layout. The biomass is dried by the excess heat of the system to a

moisture level of 25% prior to gasification, to lower the $CH_4$ content in the syngas produced. The gasifier oxidizing agent is pure $O_2$, which is generated without excess by the SOEC to maintain an equivalence ratio ER = 0.2. This yields $N_2$-free syngas which is cleaned using hot gas techniques, as they are highly recommended for such small-scale facilities since only limited waste handling is required [33]. Particulate matter (PM) is cleared using a cyclone, and tar is reformed in a steam fluidized nickel bed operating at 780 ˚C, with a steam to carbon ratio of 3. Nickel-based catalysts are used for tar decomposition primarily due to their high conversion efficiencies (>99% at 780 ˚C [34]), along with their ability to enhance the $H_2$ and CO content of syngas and reform methane [35]. The tar-free syngas is then injected into a 400˚C ZnO guard bed for acid gas adsorption [15].

To lower the compressor work, the cleaned syngas is cooled to 40 ˚C and water is separated using a flash condenser. The syngas is then enriched with $H_2$ from the SOEC before compressing it to 30 bar for MeOH synthesis. This operation is usually conducted at pressures between 60 to 80 bar [10], but as a compromise between MeOH conversion efficiency and the complications associated with higher operating pressures, a lower pressure of 30 bar is selected in this study. In the MeOH synthesis subsystem (Figure 1), the syngas is cooled to 225 ˚C and injected into an isothermal reactor with Cu/ZnO catalyst [10]. The mixture exiting the MeOH reactor is cooled to 40 ˚C and sent to a flash separator. The liquid mixture is crude MeOH, and the exiting gas stream (unreacted syngas) is sent to a SOFC operating at 850 ˚C and 1 bar. The SOFC generates a net output of electricity (Figure 1, dashed line) after powering the SOEC and the syngas compressor. The high temperature of the SOFC is maintained by heating the inlet anodic and cathodic streams using the high-temperature exhaust streams. At this stage of the process, the leftover syngas is highly diluted in $CO_2$ and $H_2O$, and is sent to a burner to exploit the remaining energy for generating steam for the nickel fluidized bed. After combustion, the exhaust gas is expected to be clean enough to be injected into a facility that requires $CO_2$ enrichment, such as a greenhouse. Further details on the operating conditions of each unit in the system can be found in section 2.4.

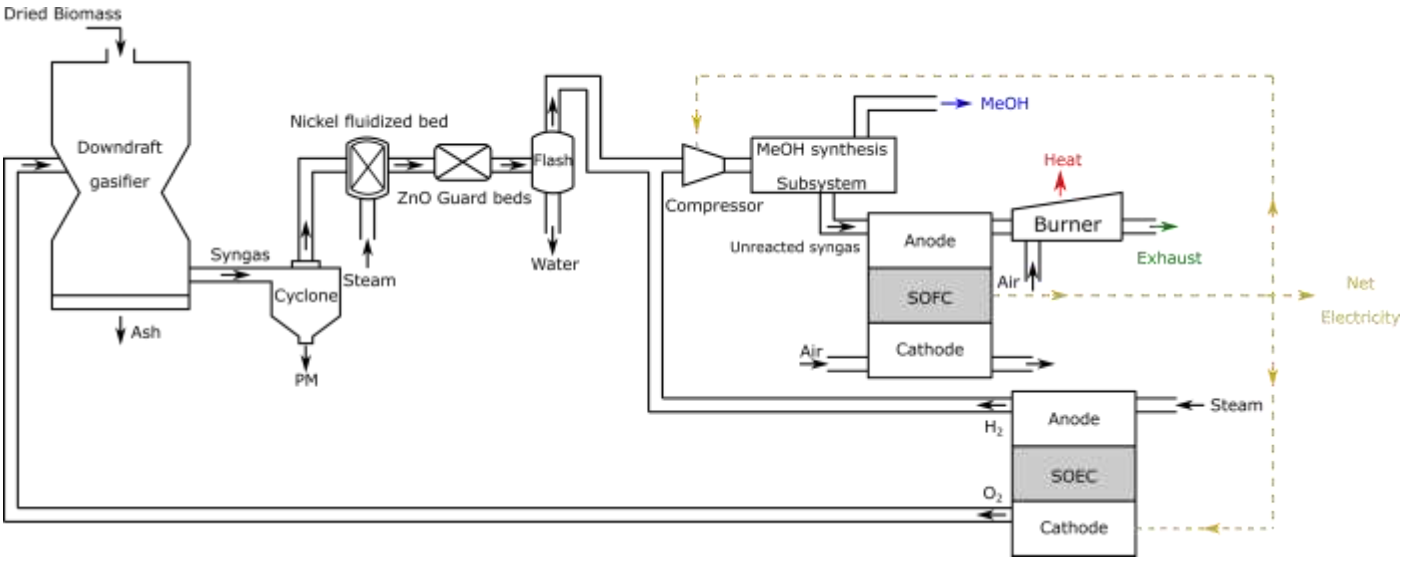


Figure 1: Simplified schematic representation of the downdraft gasifier-based system.

### 2.3. Dual fluidized bed gasifier-based system

A DFB gasifier operating at 1 bar and 850 ˚C is used in the second proposed system, shown in Figure 2. The gasification agent is steam generated using the heat from the residual gas burner. This gasification approach was developed by the Vienna University of Technology, and is sometimes referred to as fast internally circulating fluidized bed (FICFB). The dried biomass (moisture = 25%) is gasified in a bubbling fluidized bed, which operates at a steam to biomass ratio S/B = 1.5, to ensure low $CH_4$ content in the syngas. The residual char and bed material are transferred via an inclined chute to a fast circulating fluidized bed, where pure $O_2$ at 450 ˚C from the SOEC is used for oxy-fuel combustion. The combustion gases are separated in a cyclone where the hot bed material is returned to the gasifier, via a loop seal, to provide the required heat for the endothermic gasification reactions. The chute and loop seals are fluidized by steam, preventing gas leakage from the combustion zone and providing $N_2$-free syngas from the gasification chamber even if air is used as an oxidizing agent [36]. The reason motivating the use of pure $O_2$ as an oxidizing agent in the proposed system is the resulting $CO_2$-rich exhaust that has a molar purity greater than 90%, suitable for sequestration/liquefaction. This idea has been briefly introduced in the review paper of Heidenreich and Foscolo [33], but is scarcely investigated in DFB gasifier-based systems in the literature despite its potential to render the biomass conversion process carbon negative. The syngas generated from the DFB gasifier has a large heating value and $H_2$ content (high cold gas efficiency), suitable for subsequent fuel synthesis [37]. The remainder of the system

for syngas cleaning and conversion is similar to the description in section 2.2. Here again, just enough $O_2$ is generated by the SOEC to combust the char in order to sustain gasification at 850 ˚C.

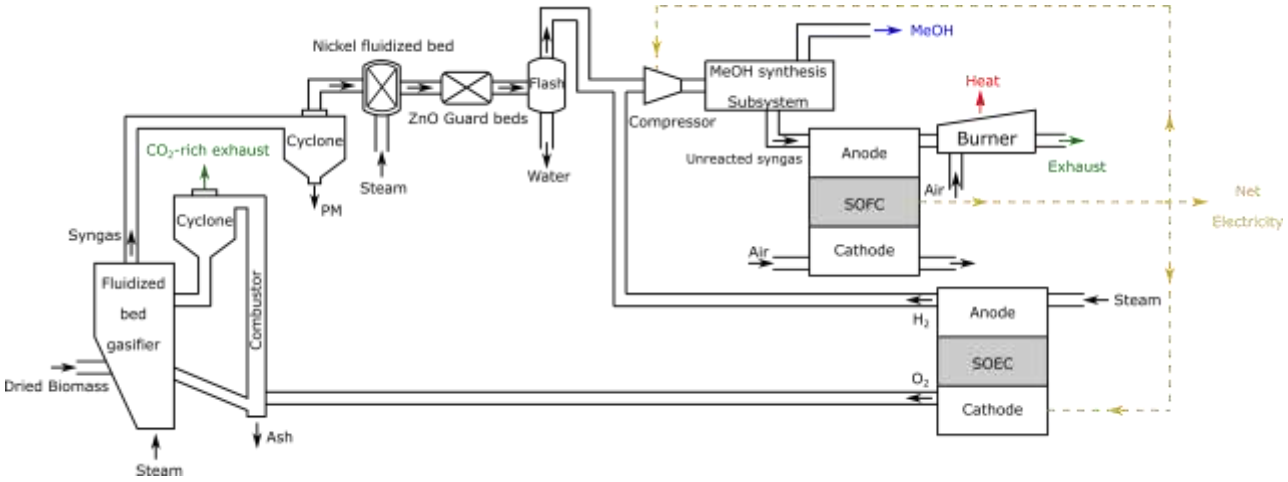


Figure 2: Simplified schematic representation of the DFB gasifier-based system.

### 2.4. Thermodynamic modelling

Thermodynamic modelling is considered a more convenient approach than a kinetics-based one for process studies and operating conditions optimization [38], since less computational resources are required, and the generated results are independent of the specific reactor design. The Aspen Plus process simulator incorporating user-defined subroutines is used to build the steady state thermodynamic models of the systems, and highlight desirable operating points through parametric studies. The Peng-Robinson equation of state is selected to obtain thermodynamic properties [25] and no pressure drops are considered in the system components [39].

The model developed by Han et al. [40] is used for the downdraft gasifier operating at 775 ˚C and with an equivalence ratio of ER = 0.2. The model relies on Gibbs free energy minimization with chemical equilibrium restrictions. This approach was successfully validated against experimental data from hardwood chips gasification [40]. The steam DFB gasifier operates at 850 ˚C with a steam to biomass ratio S/B = 1.5. It is modelled using the zero-dimensional model by Doherty et al. [41], a suitable approach as the majority of the biomass conversion takes place in the homogeneous bottom part of the gasifier. Again, this model's syngas composition, gasification temperature and carbon conversion have been validated against experimental data from wood chips gasification [41]. Tar in crude syngas is represented as 60% benzene ($C_6H_6$), 20% toluene ($C_7H_8$), and 20% naphthalene ($C_{10}H_8$) by weight [42], and its total concentration (on dry basis)

assumed at 5 g/Nm$^3$ [43] and 9.5 g/Nm$^3$ [36] for the downdraft and DFB gasifiers, respectively. For both gasifiers, 5.5% of the input biomass HHV is considered to be lost as heat in the gasification process.

The cyclones are modelled using the SSPLIT block, assumed to fully separate ash and char from syngas [44]. Tar reforming in the nickel beds is simulated in two stages [38]: First, tar is converted to CO and $H_2$ as it fully reacts at a steam to carbon ratio of 3 and 780˚C in an RSTOIC reactor according to the following equation:

$$C_xH_yO_z + (x - z)H_2O \leftrightarrow xCO + \left(\frac{y}{2} + x - z\right)H_2 \quad (1)$$

Then, the exiting stream is injected into an adiabatic RGIBBS reactor where equilibrium is attained through methane steam reforming and water-gas shift (WGS) reactions:

$$CH_4 + H_2O \leftrightarrow CO + 3H_2 \quad (2)$$

$$CO + H_2O \leftrightarrow CO_2 + H_2 \quad (3)$$

The SEP blocks are used to simulate the guard beds operating at 400 ˚C, with full acid gas removal, and a temperature drop across the bed assumed at 100 ˚C. The FLASH2 block is used for the adiabatic flash separators, and the COMPR block is used for the adiabatic compressors. The compressors discharge pressure is specified at 30 bar, with an isentropic efficiency of 80%.

An RGIBBS block operating at 225 ˚C and 30 bar is used to replicate chemical reactions 3 and 4 that occur in catalytic methanol reactor [25]:

$$CO + 2H_2 \leftrightarrow CH_3OH \quad (4)$$

Chemical equilibrium calculations with temperature approach are often used in system studies to model reactors with finite residence time, 15 ˚C is used here for both reactions [16]. For the exothermic MeOH reactions, which are favored at low temperatures, equilibrium is evaluated at temperatures slightly higher than the reactor temperature to account for non-equilibrium effects.

Figure 3 shows the Aspen Plus flowsheet used to model the SOFC. The anode's "AN-HEAT" and cathode's "CAT-HEAT" are two heat streams required to increase the temperature of the injected syngas and air flowing in the SOFC to 850 ˚C obtained from the hot exhaust gas. The SEP block "CAT" is used to separate $O_2$ from air and supply it as "O2-AN" to the anode, as in practice only

the $O_2$ content in air is conducted across the electrolyte. The required flowrate of air is determined by the fraction of the supplied fuel that reacts to produce power in the unit, also known as the utilization factor, which is set at $U_f$ = 0.7 [45]. The anode is modelled by an RGIBBS reactor "ANODE" operating at 1 bar. The reactions taken into account are the WGS reaction (Eq. 3) and that for $H_2$ oxidation [45]:

$$H_2 + \frac{1}{2}O_2 \leftrightarrow H_2O \tag{5}$$

Reactions involving $CH_4$ and $CH_3OH$ are not considered as their concentrations in the syngas stream entering the SOFC are minute ($CH_3OH$<0.7% and $CH_4$<0.05%), and also since their reforming reactions require considerably higher pressures (approximately 20 bar for $CH_4$) [17]. The operating voltage ($V_{op}$) of the SOFC is calculated from the average Nernst voltage ($V_N$) assuming a constant area specific resistance (ASR) [17,46,47] of 0.2 Ω $cm^2$ as per the following equations:

$$V_{op} = V_N - iASR \tag{6}$$

$$i = \frac{I}{A} = \frac{n_{H_2,r}(nF)}{A} \tag{7}$$

$$V_N = V^o - \frac{\Delta\hat{s}}{nF}(T - T_o) - \frac{RT}{nF}\ln\frac{\prod a_{products}^{v_i}}{\prod a_{reactants}^{v_i}} \tag{8}$$

$$V^o = -\frac{\Delta\hat{g}^o_{rxn}}{nF} \tag{9}$$

where $n_{H_2,r}$ is the number of $H_2$ moles undergoing electrochemical reactions at the anode. The active cell area (A) is chosen such that $i$ = 1 A/$cm^2$. The average molar composition of the reactants and products are used for calculating the activity of species in the products or reactants streams $a_{products}^{v_i}$ and $a_{reactants}^{v_i}$. A user-defined script with the aforementioned equations is compiled in a CALCULATOR block, which then instructs the FSPLIT block "Q-SPLIT" to divide the total enthalpy change "Q-RAW" from the "ANODE" block into an electrical stream "ELE" (equal to the calculated electrical power) and a heat stream "HEAT" (equal to the difference between the enthalpy change and electrical power).

The RSTOIC block is used to model the SOEC [45], with an operating temperature of 850 ˚C and pressure of 1 bar. The inverse of reaction (5) is used for $H_2O$ electrolysis with a fractional

conversion equal to the $U_f$ = 0.7. The amount of $H_2O$ fed into the SOEC is determined by the amount of $O_2$ required by the gasifier. Equations 6 to 9 are used to calculate the operating voltage and current of the SOEC. The ASR and active cell area were equal to the values chosen for the SOFC since the system could in theory be operated using a single reversible solid oxide cell with appropriate electrical and gas storage [47].

The combustion of leftover syngas exiting the SOFC is modelled using an adiabatic RGIBBS chemical equilibrium block at 1 bar operated with an equivalence ratio ER = 1.2. The exhaust stream is cooled to 40˚C and the thermal energy released is considered useful heat for the greenhouse.

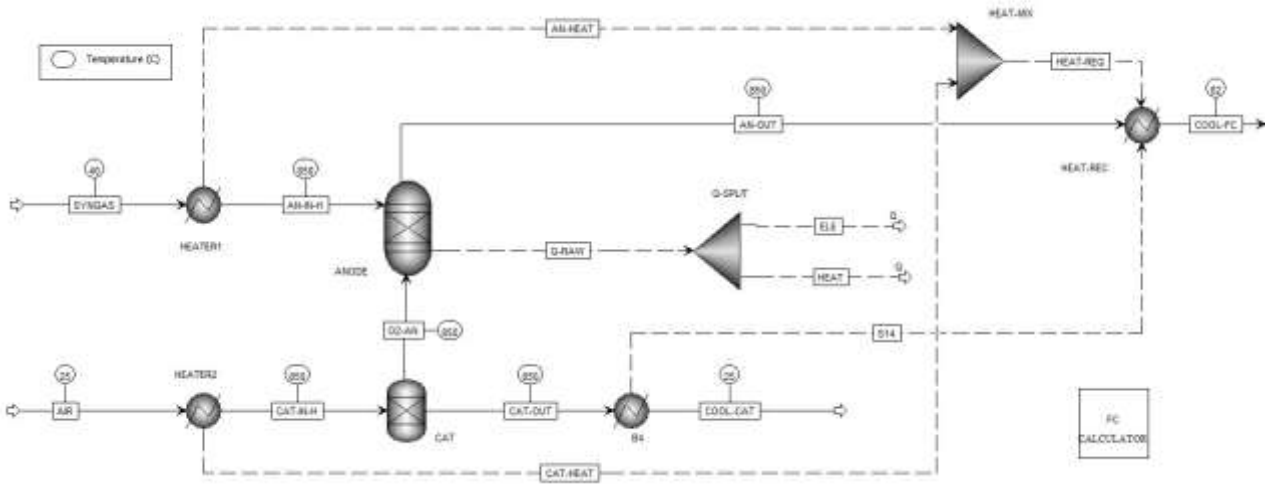


Figure 3: Aspen Plus model of the SOFC. The solid and dashed lines represent material and heat streams, respectively.

## 3. Results

To properly quantify the energetic yields, the following efficiencies are defined for the electrical, thermal, biofuel and total useful output, respectively.

$$\eta_{ele} = \frac{P_{net}}{(\dot{m}HHV)_{BM}}; \eta_{th} = \frac{\dot{Q}_{net}}{(\dot{m}HHV)_{BM}}; \eta_{biofuel} = \frac{(\dot{m}HHV)_{biofuel}}{(\dot{m}HHV)_{BM}}; \eta_{tot} = \eta_{ele} + \eta_{th} + \eta_{MeOH};$$

$\dot{m}$ is the mass flow rate of biomass input or biofuel output with a higher heating value HHV, and $P_{net}$ is the net electrical power from the SOFC after supplying the compressor and the SOEC. $\dot{Q}_{net}$ is the net thermal energy generated by the exothermic reactors and the syngas cooling stages in the system after deducting the total amount of heat required by the biomass dryer, steam generator,

and SOEC. Therefore, the sensible heat from all the cooling stages in the system, not to be confused with the system losses, is assumed to be recuperated. In practice, the number and sizes of the heat exchangers in the system must be optimized based on the overall economic returns, where a trade-off between recovering all the generated sensible heat and reducing the overall system cost/complexity may be made. As a result, the thermal and consequently overall efficiencies presented next can be thought of as the real-life upper bounds of the proposed polygeneration systems. $\eta_{ele}$, $\eta_{th}$ and $\eta_{biofuel}$ are expected to have positive values, which implies that the system does not rely on external energy sources other than biomass.

### 3.1. Downdraft gasifier-based system

#### 3.1.1. Sankey diagram and overall efficiencies

The Sankey diagram of the downdraft biomass gasifier-based system is shown in Figure 4. The operating mode described in section 2.2 ensures that the system electricity generation is maximized. As can be seen, the main energy losses occur in the drying and gasification stages, where a total of 10.7% of the input biomass energy is lost. The cold gas efficiency ($\eta_{CG}$) of the downdraft gasifier based on the lower heating value of the biomass (LHV) is 75%. Steam at 780˚C is generated from the leftover syngas burner and is added to the nickel fluidized bed reactor for tar abatement. The cleaned syngas is then enriched with $H_2$ from the SOEC for enhancing the MeOH yield, which is $\eta_{MeOH}$ = 10.3% with a $H_2$+CO conversion of 15.1%, a reasonable value considering the relatively low operating pressure.

The unreacted syngas and air that are fed to the SOFC are heated to 850 ˚C by the hot exhaust stream, which is thus cooled to 76 ˚C. The electricity yield of the SOFC is 32.3% of the system's input biomass energy, with 13.7% and 9.3% being fed to the SOEC and the syngas compressor, respectively, yielding a net electrical efficiency $\eta_{ele}$ = 9.2%. The SOFC also converts 17.1% of the input biomass energy as sensible heat, with the remaining energy (34.5%) being exploited in the unreacted syngas burner (adiabatic flame temperature of 1070 ˚C). Accounting for all useful thermal energy generated (ex: MeOH reactor, syngas cooling, syngas burner, etc.) and consumed (SOEC, steam generator, etc.), the system yields a net thermal efficiency $\eta_{th}$ = 65.1%, resulting in a total system efficiency $\eta_{tot}$ = 84.6%. Regarding the possibility of $CO_2$ greenhouse atmosphere enrichment, the burner's exhaust gas contains 0.89 kg of $CO_2$ per kg of input biomass.

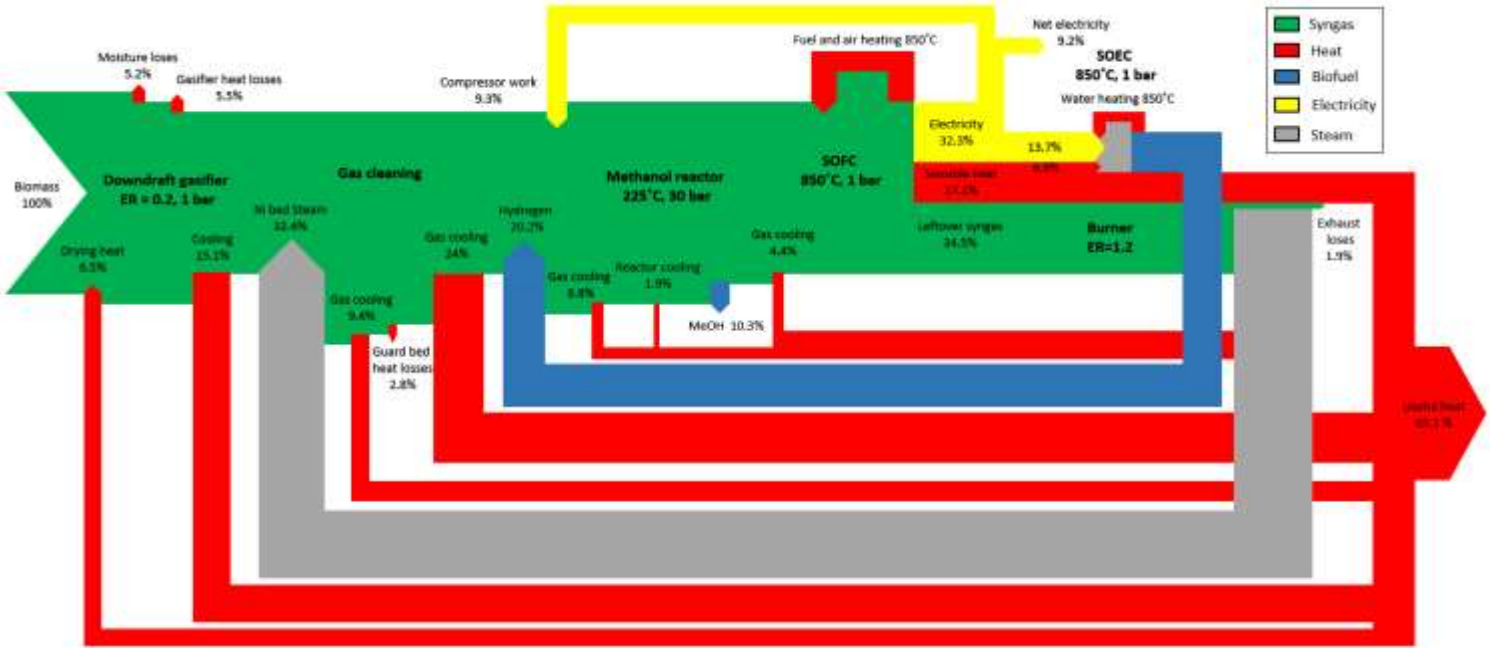


Figure 4: Sankey diagram of the downdraft gasifier-based system.

### 3.1.2. Parametric analysis

The influence of the hydrogen recycling fraction, active cell surface areas, ER and MeOH reactor pressure on the performance of the downdraft gasifier-based system has been investigated and is presented here. The $H_2$ produced by the SOEC can either be recycled to the MeOH reactor to increase its conversion efficiency, or kept as a separated stream to yield a net output ($\eta_{H_2} > 0$). Figure 5 (a) shows the variation of the system efficiencies as a function of the $H_2$ recycling fraction, defined as the ratio of the mass flowrate recycled into the MeOH reactor to the total $H_2$ generated from the SOEC. With no $H_2$ recycling ($\eta_{H_2} = 20.3\%$), the efficiency of MeOH synthesis is only $\eta_{MeOH} = 8.7\%$ at the 30 bar reference pressure considered here. This is because the $H_2$/CO ratio provided by the downdraft gasifier is approximately equal to 1, a low value for MeOH synthesis [10]. As $H_2$ starts to be injected upstream of the MeOH reactor, $\eta_{H_2}$ drops to zero, while $\eta_{MeOH}$ reaches 10.3%. The electrical and thermal outputs are increased as well, with $\eta_{tot}$ remaining approximately constant. This shows that the system is effectively converting the chemical energy of gaseous $H_2$ (produced in the SOEC) into chemical energy in liquid MeOH, electricity and heat. The corresponding conversion fractions are 9%, 18% and 73%, respectively.

The lines with markers on Figure 5 (a) show the system behavior when the active surface areas of the SOFC and SOEC are doubled. This means that the current densities are reduced by half

compared to the plain lines. This in turn improves the electrical efficiencies of both the SOFC and SOEC, and consequently, that of the system. Specifically, $\eta_{ele}$ increases by 4.2 percentage points ($\eta_{ele}$ = 13.4% at full $H_2$ recycling), with $\eta_{th}$ dropping by an equivalent amount. Hence, the loss of operating voltage and the generation of heat in the SOFC and SOEC units are reduced as expected at lower current densities.

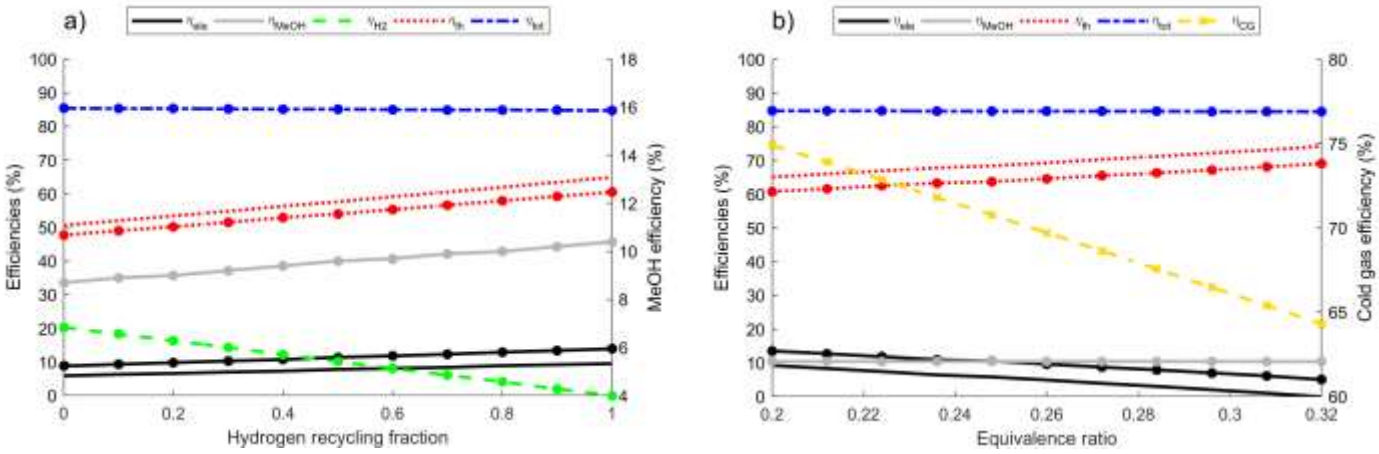


Figure 5: Variation of the downdraft gasifier-based system efficiencies with a) $H_2$ recycling fraction at ER = 0.2 and b) ER at full $H_2$ recycling. The SOFC and SOEC current densities of the lines with markers are half that of the plain ones (double of the active surface areas).

The effect of varying the equivalence ratio ER, defined as the ratio of actual $O_2$ flow rate to that required for the stoichiometric combustion of the biomass, is shown in Figure 5 (b). A minimum ER of 0.2 is considered, since lower values would result in lower gasification temperatures, and consequently higher tar concentrations in the syngas. Higher equivalence ratios are attractive for heat generation, and may be deployed when the heat demand by the greenhouse is large. The thermal efficiency is 74.2% at ER = 0.32, which is the maximum ER value that can be attained by the system without needing external electricity supply. This is because the electrical efficiency drops at higher ERs as more electricity must be consumed by the SOEC to produce more $O_2$ for the gasifier. The MeOH yield attains its peak value at ER = 0.26, and begins to slowly drop with further increase in ER since the gasifier syngas energy content becomes lower, particularly the $H_2$ concentration. This is reflected in the gasifier cold gas efficiency, which drops from $\eta_{CG}$ = 75% at ER = 0.2 to $\eta_{CG}$ = 64% at ER=0.32. Here again, the effect of doubling the active surface area of SOFC and SOEC is shown by the lines with markers. It can be seen that doing so increases the electrical efficiency $\eta_{ele}$ by 4.5 percentage points.

The effect of changing the operating pressure of the MeOH reactor is important and shown in Figure 6. These results reveal that the ER range where a net amount of electricity is generated ($\eta_{ele} > 0$) is reduced with higher operating pressures. At 70 bar, electricity must be injected into the system regardless of the value of the ER because of the increased energy demand for syngas compression. MeOH yield is considerably enhanced with high reactor pressures. At 70 bar, $\eta_{MeOH}$ = 28%, which is 2.7 times the MeOH efficiency at 30 bar. This also reduces the thermal energy output as less syngas exits the MeOH reactor unreacted, which leads to less syngas being burned. The low operating pressure chosen for the baseline cases considered here lowers $\eta_{MeOH}$, but greatly simplifies the system design and safety considerations. Also, this is compensated by the fact that other forms of useful energy are produced by the polygeneration system, where it can be seen that the high total efficiency of $\eta_{tot} = 84.6\%$ remains essentially unaffected by the operating pressure.

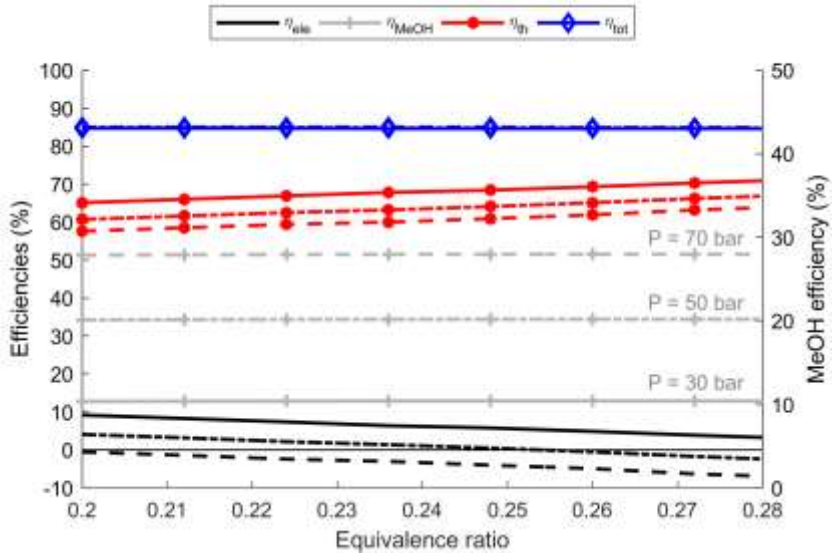


Figure 6: Efficiency of the downdraft gasifier-based system with ER at different MeOH reactor pressures (—— 30, —–— 50, and – – – 70 bar).

### 3.2. Dual fluidized bed gasifier-based system

In the second system considered, the downdraft gasifier is replaced by a steam DFB gasifier. The $O_2$ from the SOEC is this time injected into the gasifier`s combustion chamber.

#### 3.2.1. Sankey diagram and overall efficiencies

The Sankey diagram in Figure 7 shows the energy flow in the DFB gasifier-based system, with the operating mode described in section 2.3 aimed at maximizing electrical yield. 11.3% of the

input biomass energy is lost as water vapor in the dryer, as heat in the gasifier, and as hot exhaust gases from the gasifier's combustion chamber. Steam at 450 ˚C is produced by the leftover syngas burner and injected into the gasification chamber. It should be noted that the drying stage is mandatory despite adding steam into the gasifier. This is because for a given steam to biomass ratio, the total water content (steam + biomass moisture) must be considered against the dry biomass weight, the amount of fluidizing steam thus decreases with increasing biomass moisture. Hence, with a 45% moist feedstock, a drying stage is mandatory to ensure adequate fluidization. The resulting cold gas efficiency based on the LHV for the DFB is 87%. After the syngas cleaning stages, the $H_2$ content is increased using the SOEC output, with the resulting stream compressed to 30 bar and fed into the MeOH reactor, yielding $\eta_{MeOH}$ = 12.2% with a $H_2$+CO conversion of 16.6%.

The unreacted syngas from the MeOH synthesis stage is then heated by the hot exhaust stream exiting the SOFC at 850˚C, and fed into the unit for electricity generation. The SOFC generates a total electric yield equivalent to 33.9%, out of which an amount equivalent to 8.9% of the input biomass energy is fed into the SOEC, and 8.7% into the syngas compressor, resulting in a net system electricity efficiency of $\eta_{ele}$ = 16.4%. The remaining energy exiting the SOFC is in the form of sensible heat (18.7%) and chemical energy in leftover syngas (34.0%), which is burned for heat with an adiabatic flame temperature of 1420 ˚C. Accounting for all the useful thermal energy generated (ex: MeOH reactor, syngas cooling, leftover syngas burning, etc.) and consumed (biomass drying, SOEC, steam generator, etc.), the system results in a thermal efficiency of $\eta_{th}$ = 56.3 %. This leads to an overall efficiency for this DFB gasifier-based system of $\eta_{tot}$ = 84.9%.

This system has two gas streams that could be used for greenhouse atmosphere $CO_2$ enrichment. The first is the exhaust of the gasifier's combustion chamber, and the second is the exhaust of the syngas burner. The former produces 0.13 kg of $CO_2$ per kg of input biomass with a molar $CO_2$ purity that exceeds 90%. The absence of $N_2$ allows for convenient $CO_2$ liquefaction or sequestration. Hence this approach has the potential to render the biomass conversion process carbon negative. The air-blown syngas burner produces an exhaust stream with 0.79 kg of $CO_2$ per kg of input biomass at 29% molar purity.

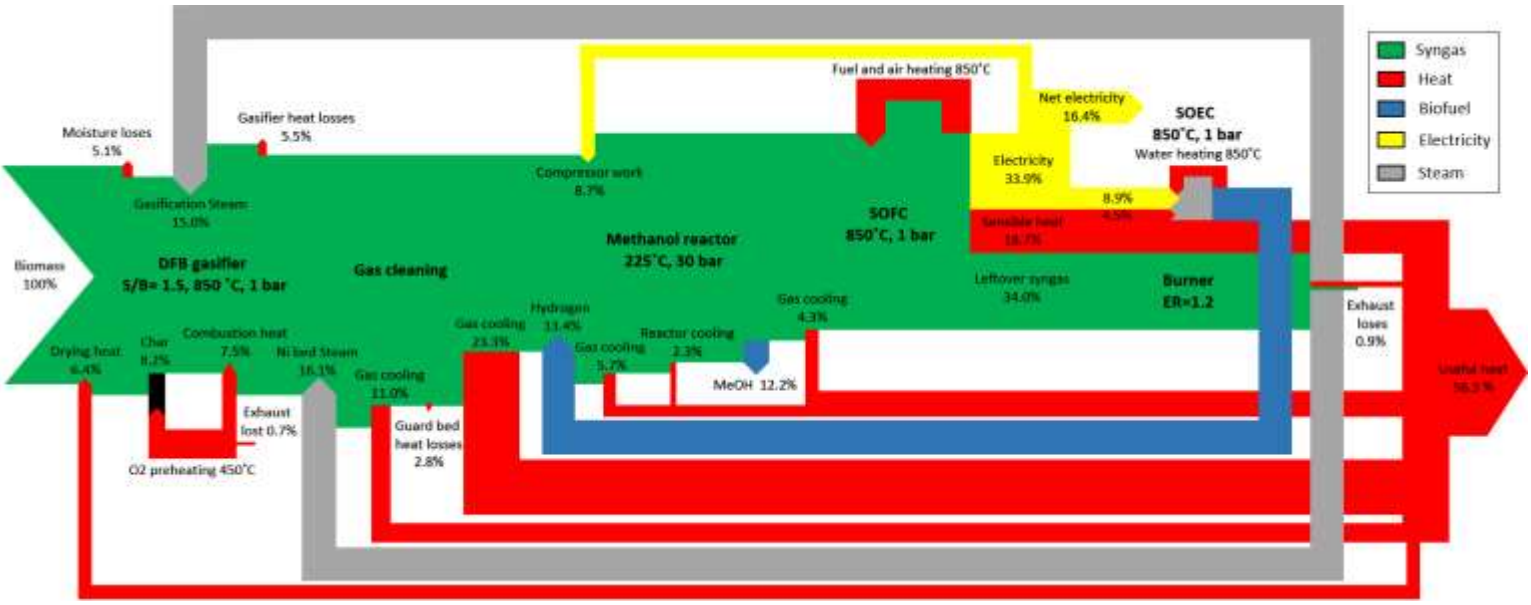


Figure 7: Sankey diagram of the DFB gasifier-based system.

### 3.2.2. Parametric analysis

The performance of the DFB gasifier-based system is shown in Figure 8 as a function of the ratio of the actual over the baseline recycled $H_2$ flow from the SOEC. The baseline case represents a $H_2$ recycling fraction (as defined in section 3.1.2) of one, where all the $H_2$ made available by the SOEC is recycled in the syngas when producing exactly the amount of $O_2$ required for the gasifier. Two zones are distinguished by shading, with their interface representing the baseline case. In the unshaded zone, the $H_2$ recycling fraction is changed between zero and one. Without $H_2$ recycling, the MeOH and electrical efficiencies drop to $\eta_{MeOH}$ = 11.1% and $\eta_{ele}$ = 13.1%. These values increase approximately linearly to $\eta_{MeOH}$ = 12.2% and $\eta_{ele}$ = 16.4% at full recycling, with the fractional conversion of $H_2$ energy into MeOH and electricity being 9.0% and 24.6%, respectively. The remaining 66.4% goes to heat.

Since at full $H_2$ recycling the electrical yield $\eta_{ele}$ is relatively high, more electricity can be sent to the SOEC to produce more $H_2$ in order to boost MeOH synthesis. The system performance under these conditions is shown in the shaded zone of Figure 8. MeOH conversion efficiency $\eta_{MeOH}$ increases from 12.2% to 14.1% when all the electricity is used to generate $H_2$. This results in a 3.5% increase in the mass flow rate into the reactor. If the active areas of the SOFC and SOEC units are doubled from the reference case (SOFC current density of 1 A/cm$^2$), the MeOH

conversion efficiency $\eta_{MeOH}$ can reach 15%, with a 5.7% increase in the mass flow rate into the MeOH reactor relative to the baseline case (lines with markers in Figure 8). In the shaded zone, the system converts 12% of the electrical energy to chemical energy in MeOH, and the remainder to thermal energy. A steam to biomass ratio S/B = 1.5 is maintained throughout, implying that an excess pure $O_2$ stream is generated by the system in the shaded zone which can be useful for other purposes. It should be noted that the amount of $O_2$ fed into the gasifier`s combustor is linked to the S/B ratio. This is because at higher S/B ratios, more char is required to be burned in the combustor to sustain the gasification temperature, and hence, more $O_2$ is needed. Figure 8 also reveals that MeOH synthesis is always increased with more $H_2$ enrichment. To determine the optimal operating point, the change in the size of the MeOH reactor, as well as the expenses and benefits of using or storing $H_2$ must be taken into account. This example reveals the usefulness of these parametric studies to investigate the flexibility of the system to respond to different demands.

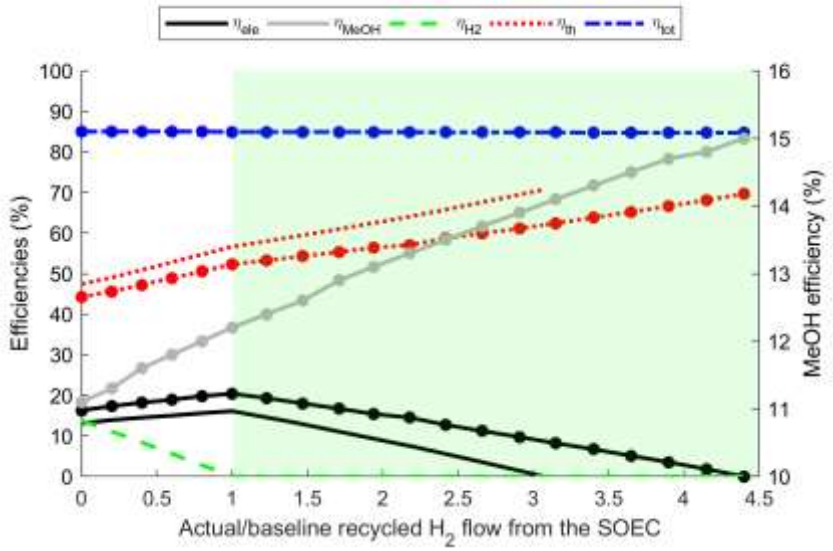


Figure 8: Variation of the DFB gasifier-based system performance as a function of the ratio of the actual over the baseline recycled $H_2$ flow from the SOEC. The SOFC and SOEC current densities of the lines with markers are half that of the plain ones (double the active surface areas).

The maximum amount of electricity generated by the second system ($\eta_{ele}$ = 16.4%) is significantly greater than that of the first system ($\eta_{ele}$ = 9.2%). Hence, a greater fraction of the unreacted syngas may be sent directly to the burner instead of the SOFC if heat is the most desirable output for the greenhouse. The performance of the second system with different amounts of unreacted syngas being sent to the SOFC is shown in Figure 9. When the amount of syngas sent to the SOFC is

sufficient for it to only power the SOEC and compressor ($\eta_{ele} = 0\%$), the system thermal efficiency attains a peak value of $\eta_{th} = 71.7\%$.

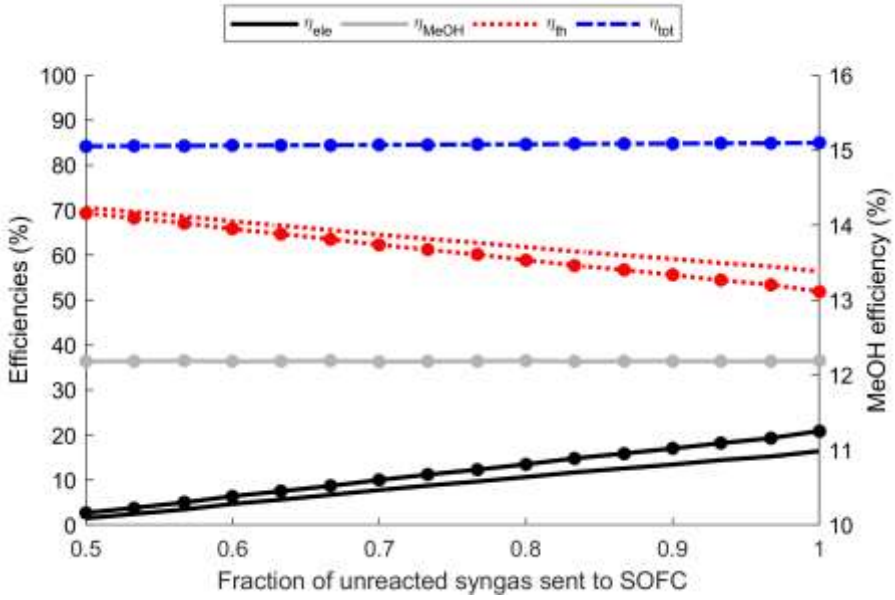


Figure 9: Variation of the DFB gasifier-based system performance as a function of the unreacted syngas sent to the SOFC. The SOFC and SOEC current densities of the lines with markers are half that of the plain ones (double the active surface areas).

The effect of changing the MeOH reactor pressure is shown in Figure 10. For the default case of 30 bar, $\eta_{MeOH} = 12.2\%$. With increasing pressure, more MeOH is synthesized from syngas, and $\eta_{MeOH}$ increases to 30.9% at 70 bar. At this pressure, $\eta_{ele} = 6.3\%$. This excess electricity can be sent to the SOEC to generate more $H_2$ to further increase the MeOH synthesis. Doing so results in a maximum $\eta_{MeOH} = 32.4\%$ (lines with markers). Similar to the first polygeneration system, it can be seen that the total efficiency of this system remains high at $\eta_{total} = 84.9\%$ and unaffected by the operating pressure.

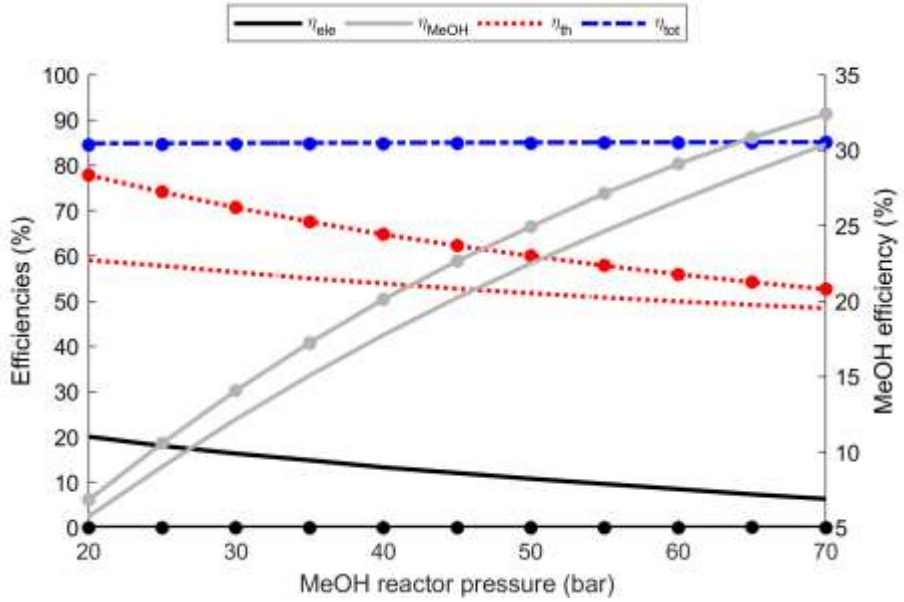


Figure 10: Effect of changing the MeOH reactor pressure. The lines with markers represent full depletion of electricity to maximize $H_2$ enrichment.

## 4. System comparison and discussion

To compare the performances of both systems, four cases are considered, each aiming to maximize a different form of energy, as can be seen in Table 2 and Table 3, with the results summarized in Figure 11. In the following, $H_{2,rec}$ denotes the $H_2$ recycling fraction defined earlier (abscissa of Figure 5 (a)). The parameter SOFC split represents the fraction of unreacted syngas sent to the SOFC in the DFB gasifier-based system (abscissa of Figure 9) with the rest sent directly to the burner. Finally, $H_{2,actual}/H_{2,baseline}$ is the ratio defined earlier of the actual over the baseline recycled $H_2$ flow from the SOEC (abscissa of Figure 8).

Case 1 for both systems represents the baseline configuration discussed in sections 2.2 and 2.3, and aims to maximize electricity generation. Under those conditions, the maximum $\eta_{ele}$ of the second system is approximately seven percentage points greater than that of the first. The main reason for this difference is that the downdraft gasifier requires a considerably greater amount of $O_2$ (approximately 1.5 times) compared to the DFB gasifier. This means that more electricity is consumed by the SOEC, thereby lowering the net electrical yield of the first system. Case 2 aims at maximizing the MeOH yield. Due to the higher $H_2$ content in the syngas generated using the DFB gasifier relative to the downdraft gasifier, the maximum $\eta_{MeOH}$ for the second system is three percentage points greater. The yield is ultimately limited in both systems by the operating pressure

of the MeOH reactor (30 bar) as discussed previously. Similarly in case 3, where the $H_2$ yield is maximized, the second system is more than five percentage points more efficient than the first. For the final case, the maximum thermal efficiency of the downdraft gasifier-based system is slightly greater than the DFB-based configuration since in the latter, more syngas is converted to MeOH, and less of it is sent to the downstream exothermic components.

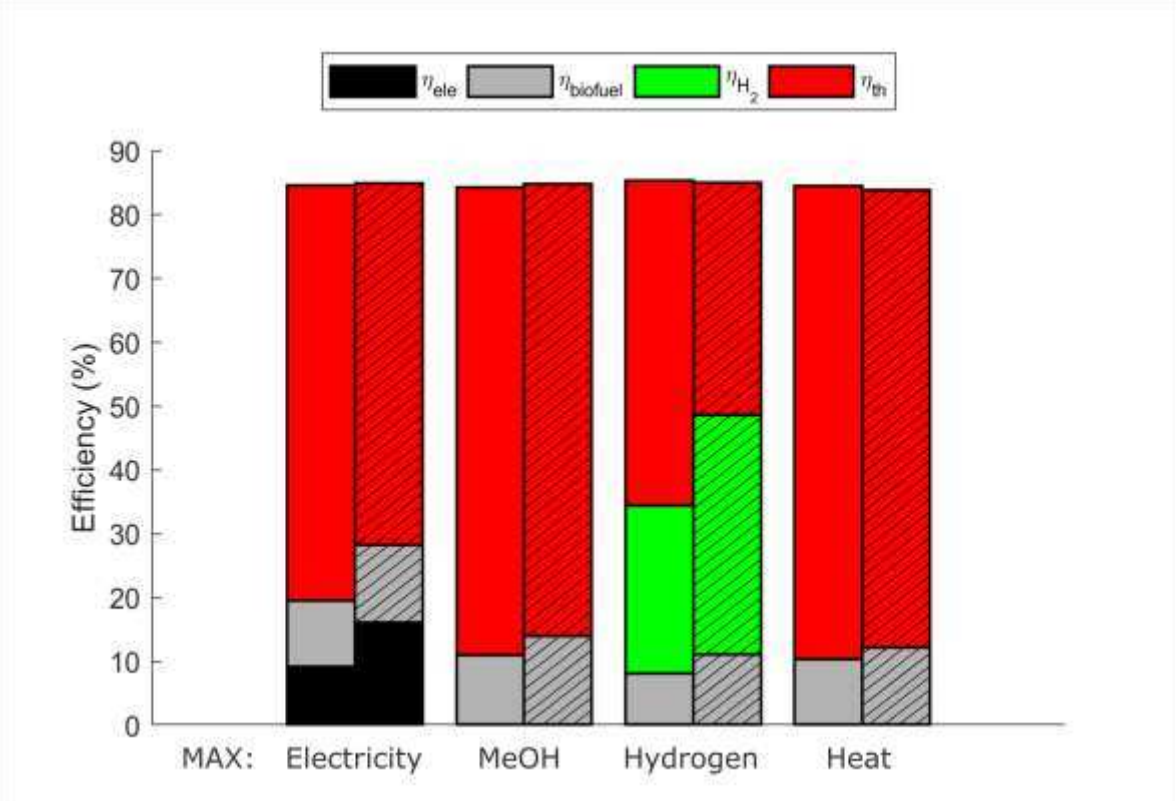


Figure 11: Performances of the downdraft gasifier-based system (plain) and the DFB gasifier-based system (hatched) under different conditions (Table 2 and Table 3).

**Table 2: Different operating conditions of the downdraft gasifier-based system with a MeOH reactor pressure of 30 bar.**

| *Case #* | *Objective* | *ER* | $H_2$*,rec* | $\eta_{ele}$ | $\eta_{MeOH}$ | $\eta_{H_2}$ | $\eta_{th}$ | $\eta_{tot}$ |
|---|---|---|---|---|---|---|---|---|
| *1* | Maximizing electricity | 0.2 | 100% | 9.2% | 10.3% | 0% | 65.1% | 84.6% |
| *2* | Maximizing MeOH | 0.26 | 100% | 0% | 11.0% | 0% | 73.6% | 84.6% |
| *3* | Maximizing $H_2$ | 0.26 | 0% | 0% | 8.2% | 26.3% | 50.9% | 85.4% |
| *4* | Maximizing heat | 0.32 | 100% | 0% | 10.3% | 0% | 74.2% | 84.5% |

**Table 3: Different operating conditions of the DFB gasifier-based system with a MeOH reactor pressure of 30 bar.**

| *Case #* | *Objective* | *SOFC split* | $H_{2,actual}/H_{2,baseline}$ | $\eta_{ele}$ | $\eta_{MeOH}$ | $\eta_{H_2}$ | $\eta_{th}$ | $\eta_{tot}$ |
|---|---|---|---|---|---|---|---|---|
| *1* | Maximizing electricity | 100% | 1 | 16.1% | 12.2% | 0% | 56.6% | 84.9% |
| *2* | Maximizing MeOH | 100% | 2.8 | 0% | 14.1% | 0% | 70.8% | 84.9% |
| *3* | Maximizing $H_2$ | 100% | 0 | 0% | 11.1% | 31.9% | 42.0% | 85.0% |
| *4* | Maximizing heat | 43% | 1 | 0% | 12.2% | 0% | 71.7% | 83.9% |

## 5. Conclusion

In this paper, thermodynamic models are presented for two novel gasification-based systems capable of producing from wood chips the four main products required by greenhouses. The main difference between the two systems is in the gasification step, where the first system relies on a downdraft gasifier, while the second one uses a DFB gasifier to generate syngas. The remainder of the conversion process is similar, with the cleaned syngas supplied to a MeOH reactor at 30 bar. The unreacted syngas from the MeOH reactor is then injected into a SOFC which powers a SOEC and the syngas compressor, while generating a net output of electricity. The SOEC is used to produce $O_2$ for the gasifier, and $H_2$ for syngas enrichment. The remaining depleted syngas is burned to extract its remaining energy as heat.

Steady state thermodynamic simulations show that electricity, MeOH, heat, and $CO_2$ can be simultaneously generated by the polygeneration systems at high overall efficiencies above 83.9% despite operating the MeOH reactors at relative low pressures. The systems are aimed at small-scale decentralized implementation, where low-pressure catalytic biofuel reactors are preferred for safety reasons. This choice is clearly the limiting factor for the maximum MeOH conversion efficiency, which is higher for the DFB gasifier-based system at 14.1% relative to the downdraft gasifier-based configuration at 11.0%. Increasing the pressure from 30 to 70 bar yields almost three times more MeOH in both systems.

Comparing the other energetic yields of the two systems through parametric analyses further highlights the thermodynamic superiority of the DFB gasifier-based configuration. This approach yields higher maximum electrical and hydrogen efficiencies of 16.1% and 31.9%, respectively,

greater than those of the downdraft gasifier-based system at 9.2% and 26.3%, respectively. In addition, the system relying on a DFB gasifier provides 0.13 kg of $CO_2$ per kg of biomass input in a $N_2$-free stream with a molar $CO_2$ purity exceeding 90%. This can be readily liquefied or sequestered meaning that the process could effectively behave as a carbon capture and storage medium.

After revealing the thermodynamic feasibility of the proposed systems in this paper, future techno-economic studies will involve transient systems simulations to properly integrate and optimize the systems in agricultural settings. Temporal consumption data of heat, electricity, fuel, and $CO_2$ of a typical greenhouse will be used, and proper energy storage mediums will be incorporated in the systems to ensure that the greenhouse demands are always met. The number and sizes of the heat exchangers in the systems will be optimized based on the overall economic returns, where a trade-off must be made between recuperating all the available sensible heat, and reducing the overall systems complexity. Also, the sensitivity of the systems efficiencies with different types of agricultural biomass feedstock will be investigated. Finally, the technical challenges associated with DFB gasifiers [36] will be addressed to ultimately decide which configuration, between the two proposed systems, to adopt in an agricultural greenhouse.

## 6. Acknowledgements

The authors are grateful for the funders of this work: the Trottier Energy Institute (Trottier scholarship and project grant) and the Natural Sciences and Engineering Research Council of Canada (NSERC), [PGSD3 - 546588 - 2020].

**Nomenclature**

| | |
|---|---|
| A: | Active cell area |
| $a_{p/r}^{v_i}$: | Activity of species *i* in products or reactants |
| AGR: | Acid gas recovery |
| ASR: | Area specific resistance |
| ASU: | Air separation unit |
| BM: | Biomass |
| CHP: | Combined heat and power |
| DFB: | Dual fluidized bed |
| DME: | Dimethyl ether |
| ER: | Equivalence ratio |
| F: | Faraday's constant |
| FC: | Fixed carbon |
| FICFB: | Fast internally circulating fluidized bed |
| HHV: | Higher heating value |
| *i:* | Current density |
| I: | Generated current |
| ICE: | Internal combustion engine |
| LHV: | Lower heating value |
| $\dot{m}$: | Mass flow rate |
| MeOH: | Methanol |
| MGT: | Micro gas turbine |
| n: | Number of moles of electrons transferred |

$n_{H_2,r}$: Number of $H_2$ moles undergoing electrochemical reactions

PM: Particulate matter

RSOC: Reversible solid oxide cell

S/B: Steam to biomass ratio

SOEC: Solid oxide electrolysis cell

SOFC: Solid oxide fuel cell

$V_N$: Reversible cell voltage

$V^o$: Standard-state reversible cell voltage

$V_{op}$: Operational voltage

VM: Volatile matter

$U_f$: Fuel utilization factor

WGS: Water gas shift

$\eta_i$: Efficiency of energy form *i*={total, net electrical, thermal, biofuel}

**References**


[1] T. Yildirim, T. Bilyea, D. Buckingham, Clean Growth in Agriculture, 2019.

[2] Statistics Canada, Report on Energy Supply and Demand in Canada, 2019.

[3] M.S. Ahamed, H. Guo, K. Tanino, Energy saving techniques for reducing the heating cost of conventional greenhouses, Biosyst. Eng. (2019). doi:10.1016/j.biosystemseng.2018.10.017.

[4] Energy Fact Book 2020-2021 by Natural Resources Canada, 2020.

[5] Y. Li, Y. Ding, D. Li, Z. Miao, Automatic carbon dioxide enrichment strategies in the greenhouse: A review, Biosyst. Eng. 171 (2018) 101–119. doi:10.1016/J.BIOSYSTEMSENG.2018.04.018.

[6] L.-M. Dion, M. Lefsrud, V. Orsat, C. Cimon, Biomass Gasification and Syngas Combustion for Greenhouse CO2 Enrichment, BioResources. 8 (2013) 1520–1538.

[7] V. Dhyani, T. Bhaskar, A comprehensive review on the pyrolysis of lignocellulosic biomass, Renew. Energy. (2018). doi:10.1016/j.renene.2017.04.035.

[8] J. Chau, T. Sowlati, S. Sokhansanj, F. Preto, S. Melin, X. Bi, Techno-economic analysis of wood biomass boilers for the greenhouse industry, Appl. Energy. 86 (2009) 364–371. doi:10.1016/J.APENERGY.2008.05.010.

[9] K. Jana, A. Ray, M.M. Majoumerd, M. Assadi, S. De, Polygeneration as a future sustainable energy solution – A comprehensive review, Appl. Energy. 202 (2017) 88–111. doi:10.1016/J.APENERGY.2017.05.129.

[10] J.-P. Lange, Methanol synthesis: a short review of technology improvements, Catal. Today. 64 (2001) 3–8. doi:10.1016/S0920-5861(00)00503-4.

[11] V.S. Sikarwar, M. Zhao, P.S. Fennell, N. Shah, E.J. Anthony, Progress in biofuel production from gasification, Prog. Energy Combust. Sci. 61 (2017) 189–248. doi:10.1016/j.pecs.2017.04.001.

[12] M. Villarini, E. Bocci, A. Di Carlo, E. Savuto, V. Pallozzi, The Case Study of an Innovative Small Scale Biomass Waste Gasification Heat and Power Plant Contextualized in a Farm,

Energy Procedia. 82 (2015) 335–342. doi:10.1016/J.EGYPRO.2015.11.790.

[13] L.I. Chaves, M.J. da Silva, S.N.M. de Souza, D. Secco, H.A. Rosa, C.E.C. Nogueira, E.P. Frigo, Small-scale power generation analysis: Downdraft gasifier coupled to engine generator set, Renew. Sustain. Energy Rev. 58 (2016) 491–498. doi:10.1016/J.RSER.2015.12.033.

[14] H.R. Sara, B. Enrico, V. Mauro, D.C. Andrea, N. Vincenzo, Techno-economic Analysis of Hydrogen Production Using Biomass Gasification -A Small Scale Power Plant Study, Energy Procedia. 101 (2016) 806–813. doi:10.1016/J.EGYPRO.2016.11.102.

[15] R. Sadegh-Vaziri, M.U. Bäbler, Providing sulfur free syngas to a fuel cell system, Energy Procedia. 159 (2019) 448–453. doi:10.1016/J.EGYPRO.2018.12.041.

[16] L.R. Clausen, B. Elmegaard, J. Ahrenfeldt, U. Henriksen, Thermodynamic analysis of small-scale dimethyl ether (DME) and methanol plants based on the efficient two-stage gasifier, Energy. 36 (2011) 5805–5814. doi:10.1016/J.ENERGY.2011.08.047.

[17] L.R. Clausen, G. Butera, S.H. Jensen, High efficiency SNG production from biomass and electricity by integrating gasification with pressurized solid oxide electrolysis cells, Energy. 172 (2019) 1117–1131. doi:10.1016/J.ENERGY.2019.02.039.

[18] S.K. Sansaniwal, K. Pal, M.A. Rosen, S.K. Tyagi, Recent advances in the development of biomass gasification technology: A comprehensive review, Renew. Sustain. Energy Rev. 72 (2017) 363–384. doi:10.1016/j.rser.2017.01.038.

[19] G. Bozzano, F. Manenti, Efficient methanol synthesis: Perspectives, technologies and optimization strategies, Prog. Energy Combust. Sci. 56 (2016) 71–105. doi:10.1016/J.PECS.2016.06.001.

[20] L. Carvalho, E. Furusjö, K. Kirtania, E. Wetterlund, J. Lundgren, M. Anheden, J. Wolf, Techno-economic assessment of catalytic gasification of biomass powders for methanol production, Bioresour. Technol. 237 (2017) 167–177. doi:10.1016/J.BIORTECH.2017.02.019.

[21] N.S. Shamsul, S.K. Kamarudin, N.A. Rahman, N.T. Kofli, An overview on the production of bio-methanol as potential renewable energy, Renew. Sustain. Energy Rev. 33 (2014)

578–588. doi:10.1016/j.rser.2014.02.024.

[22] G. Butera, S. Højgaard Jensen, R. Østergaard Gadsbøll, J. Ahrenfeldt, L. Røngaard Clausen, Flexible biomass conversion to methanol integrating solid oxide cells and TwoStage gasifier, Fuel. 271 (2020) 117654. doi:https://doi.org/10.1016/j.fuel.2020.117654.

[23] L.E. Lücking, Methanol Production from Syngas Process modelling and design utilising biomass gasification and integrating hydrogen supply, Delft University of Technology, 2017. http://repository.tudelft.nl/. (accessed August 4, 2019).

[24] S.K. Aggarwal, D. Bongiovanni, M. Santarelli, Extinction of laminar diffusion flames burning the anodic syngas fuel from solid oxide fuel cell, Int. J. Hydrogen Energy. 40 (2015) 7214–7230. doi:10.1016/J.IJHYDENE.2015.04.015.

[25] H. Zhang, L. Wang, F. Maréchal, U. Desideri, Solid-oxide electrolyzer coupled biomass-to-methanol systems, Energy Procedia. 158 (2019) 4548–4553. doi:10.1016/J.EGYPRO.2019.01.755.

[26] G. Butera, S. Højgaard Jensen, R. Østergaard Gadsbøll, J. Ahrenfeldt, L. Røngaard Clausen, Biomass Conversion to Methanol Integrating Solid Oxide Cells and Two-Stage Gasifier: Effects of Carbon Dioxide Recirculation and Pressurized Operation, 76 (2019) 1177–1182. doi:10.3303/CET1976197.

[27] C. Bao, Y. Wang, D. Feng, Z. Jiang, X. Zhang, Macroscopic modeling of solid oxide fuel cell (SOFC) and model-based control of SOFC and gas turbine hybrid system, Prog. Energy Combust. Sci. 66 (2018) 83–140. doi:10.1016/J.PECS.2017.12.002.

[28] A. Baldinelli, G. Cinti, U. Desideri, F. Fantozzi, Biomass integrated gasifier-fuel cells: Experimental investigation on wood syngas tars impact on NiYSZ-anode Solid Oxide Fuel Cells, Energy Convers. Manag. 128 (2016) 361–370. doi:10.1016/J.ENCONMAN.2016.09.048.

[29] M. Skrzypkiewicz, M. Wierzbicki, M. Stępień, Solid Oxide Fuel Cells coupled with a biomass gasification unit, E3S Web Conf. 10 (2016) 1–5. doi:10.1051/e3sconf/20161000115.

[30] R.Ø. Gadsbøll, A. Vivar Garcia, J. Ahrenfeldt, U.B. Henriksen, Solid oxide fuel cell stack

coupled with an oxygen-blown TwoStage gasifier using minimal gas cleaning, Renew. Energy. 139 (2019) 1255–1262. doi:10.1016/J.RENENE.2019.03.038.

[31] M. Minutillo, A. Perna, E. Jannelli, V. Cigolotti, S.W. Nam, S.P. Yoon, B.W. Kwon, Coupling of Biomass Gasification and SOFC – Gas Turbine Hybrid System for Small Scale Cogeneration Applications, Energy Procedia. 105 (2017) 730–737. doi:10.1016/J.EGYPRO.2017.03.383.

[32] A.A.P. Susastriawan, H. Saptoadi, Purnomo, Small-scale downdraft gasifiers for biomass gasification: A review, Renew. Sustain. Energy Rev. 76 (2017) 989–1003. doi:10.1016/J.RSER.2017.03.112.

[33] S. Heidenreich, P.U. Foscolo, New concepts in biomass gasification, Prog. Energy Combust. Sci. 46 (2015) 72–95. doi:10.1016/j.pecs.2014.06.002.

[34] R. Zhang, R.C. Brown, A. Suby, K. Cummer, Catalytic destruction of tar in biomass derived producer gas, Energy Convers. Manag. 45 (2004) 995–1014. doi:10.1016/j.enconman.2003.08.016.

[35] A. Kostyniuk, M. Grilc, B. Likozar, Catalytic Cracking of Biomass-Derived Hydrocarbon Tars or Model Compounds To Form Biobased Benzene, Toluene, and Xylene Isomer Mixtures, (2019). doi:10.1021/acs.iecr.9b01219.

[36] N. Hanchate, S. Ramani, C.S. Mathpati, V.H. Dalvi, Biomass gasification using dual fluidized bed gasification systems: A review, J. Clean. Prod. 280 (2021). doi:10.1016/j.jclepro.2020.123148.

[37] S. Fendt, A. Tremel, M. Gaderer, H. Spliethoff, The potential of small-scale SNG production from biomass gasification, Biomass Conv. Bioref. 2 (2012) 275–283. doi:10.1007/s13399-012-0037-3.

[38] T. Gröbl, H. Walter, M. Haider, Biomass steam gasification for production of SNG – Process design and sensitivity analysis, Appl. Energy. 97 (2012) 451–461. doi:10.1016/J.APENERGY.2012.01.038.

[39] P.-C. Kuo, W. Wu, W.-H. Chen, Gasification performances of raw and torrefied biomass in a downdraft fixed bed gasifier using thermodynamic analysis, Fuel. 117 (2014) 1231–1241.

doi:10.1016/J.FUEL.2013.07.125.

[40] J. Han, Y. Liang, J. Hu, L. Qin, J. Street, Y. Lu, F. Yu, Modeling downdraft biomass gasification process by restricting chemical reaction equilibrium with Aspen Plus, Energy Convers. Manag. (2017) 641–648. doi:10.1016/j.enconman.2017.10.030.

[41] W. Doherty, A. Reynolds, D. Kennedy, W. Doherty, A. Reynolds, D. Kennedy, Aspen Plus Simulation of Biomass Gasification in a Steam Blown Dual Fluidised Bed, in: Mater. Process. Energy, 2013.

[42] T. Damartzis, S. Michailos, A. Zabaniotou, Energetic assessment of a combined heat and power integrated biomass gasification–internal combustion engine system by using Aspen Plus®, Fuel Process. Technol. 95 (2012) 37–44. doi:10.1016/J.FUPROC.2011.11.010.

[43] L. Yuping, L. Chen, T. Wang, L. Ma, M. Ding, X. Zhang, X. Yin, Demonstration of Pilot-scale Bio-dimethyl ether Synthesis Via Oxygen- and steam- enriched Gasification of Wood Chips, in: Energy Procedia, Elsevier, 2015: pp. 202–207. doi:10.1016/J.EGYPRO.2015.07.303.

[44] M.C. Acar, Y.E. Böke, Simulation of biomass gasification in a BFBG using chemical equilibrium model and restricted chemical equilibrium method, Biomass and Bioenergy. 125 (2019) 131–138. doi:10.1016/J.BIOMBIOE.2019.04.012.

[45] M. Hauck, S. Herrmann, H. Spliethoff, Simulation of a reversible SOFC with Aspen Plus, Int. J. Hydrogen Energy. 42 (2017) 10329–10340. doi:10.1016/J.IJHYDENE.2017.01.189.

[46] S. Mesfun, J. Lundgren, A. Toffolo, G. Lindbergh, C. Lagergren, K. Engvall, Integration of an electrolysis unit for producer gas conditioning in a bio-synthetic natural gas plant, J. Energy Resour. Technol. Trans. ASME. 141 (2019) 1–12. doi:10.1115/1.4040942.

[47] G. Butera, S.H. Jensen, L.R. Clausen, A novel system for large-scale storage of electricity as synthetic natural gas using reversible pressurized solid oxide cells, Energy. 166 (2019) 738–754. doi:10.1016/J.ENERGY.2018.10.079.